Appl. Phys. A (2014) 117:1249–1258
DOI 10.1007/s00339-014-8513-1

Applied Physics A
Materials Science & Processing

Stable and luminescent wurtzite CdS, ZnS and CdS/ZnS core/shell quantum dots

Hitanshu Kumar · Manoj Kumar · P. B. Barman · Ragini Raj Singh

Received: 24 February 2014 / Accepted: 12 May 2014 / Published online: 6 June 2014

Abstract This article presents first report on the highly stable and luminescent wurtzite CdS, ZnS and CdS/ZnS quantum dots (QDs) where the role of precursor selection at room temperature is the key. X-ray diffraction (XRD), optical absorbance spectroscopy, photoluminescence spectroscopy, Fourier transform infrared spectroscopy and transmission electron microscopy have been employed in order to characterize these QDs. XRD indicates the formation of wurtzite CdS, ZnS and CdS/ZnS system. Broadening in XRD peaks revealed the reduction in particle size such as 4.2, 5.2 and 5.8 nm for CdS, ZnS and CdS/ZnS, respectively, compared to their bulk counterparts. Blue shift in absorbance has been observed in each case as particles size decreases. The photoluminescence intensity emission of CdS/ZnS core/shell was strongly superior from that observed in individual CdS and ZnS nanoparticles. We also propose that the core and shell interface leads to favourable conditions that instigate photoluminescence emission in CdS/ZnS core/shell system. One notable result of this work obtained from the photoluminescence analysis is the significant reduction in full width at half maxima, in emission peak of core/shell structure which shows the enhanced monochromaticity. We have found that OH, CH_2 and C–O functional groups are present on the QDs surface and that is why these QDs can be easily attachable to biomolecules. TEM analysis has been employed for confirmation of particle size and found to be 5.3, 5.8 and 6.2 nm for CdS, ZnS and CdS/ZnS structures, respectively.

H. Kumar · P. B. Barman · R. R. Singh (✉)
Department of Physics and Materials Science,
Jaypee University of Information Technology, Waknaghat,
Solan 173234, HP, India
e-mail: raginirajsingh@gmail.com

M. Kumar
Department of Physics and Materials Science,
Jaypee Institute of Information Technology,
A-10 Sector-62, Noida 201 307, Uttar Pradesh, India

1 Introduction

Stability of QDs was of paramount importance as it will give consistent luminescence after a span of time and in different conditions. There is a demand for these stable luminescent QDs specifically in bio-imaging applications. The emission colour from semiconductor nanocrystal quantum dots is tunable by the size [1–4]. In the case of semiconductor nanoparticles, radiative or nonradiative recombination of an exciton at the surface states becomes dominant in its optical properties with a decrease in particle size and it is very useful in solar energy conversion, light-emitting devices, chemical/biological sensors, biolabelling [5–7] and photo-catalysis [8–12] which imposes stringent requirements of a high-fluorescence quantum yield (QY), and of high stability against photo-degradation. These characteristics are difficult to achieve in semiconductor nanocrystals coated by organic ligands due to imperfect surface passivation. In addition, the organic ligands are liable for exchange reactions because of their weak bonding to the nanocrystal surface atoms [13]. Growing an epitaxial shell of a wide band gap semiconductor around a nanocrystal core is a proven strategy for increasing both the stability to photo-oxidation and the photoluminescence quantum yield (PLQY) [14, 15].

Effects of precursors on the crystal structure and photoluminescence (PL) of CdS and ZnS have been studied [16 and references therein], and these works show that the crystal structure, particle size and PL of CdS and ZnS

nanoparticles frequently varied with the factors such as precursors, stabilizer, solvent effect and synthesis methods. However, mostly spherical, uniform and wurtzite nanoparticles were synthesized by high-temperature methods such as hydrothermal microemulsion where the obtained particle sizes were from 20 to 80 nm [17]. In this work, the synthesis and characterisation of 2-mercaptoethanol capped wurtzite zinc sulphide (ZnS), cadmium sulphide (CdS) and their core/shell QD structures (CdS/ZnS) by wet chemical method have been presented. We have synthesized and reported first time the wurtzite structures at room temperature. We have selected the precursors on the basis of previously reported results in order to obtain wurtzite structures specifically near room temperature as room-temperature wurtzite quantum dots possess small sizes with excellent optical properties and the wurtzite phase is more stable. CdS/ZnS core/shell structures were formed by capping of CdS core, with a thin ZnS shell. ZnS has a wider band gap than CdS, which allows the epitaxial growth of a thin ZnS layer outside the CdS core. Wet chemical method is widely used for the preparation of colloidal nanoparticles because of its several advantages such as inexpensive raw materials, easy handling and capability of producing high-purity samples; also, the agglomeration is less compared to the other methods [18]; and they form particles of much smaller size with higher surface area than those reported by other methods. CdS/ZnS quantum dots are biocompatible due to the use of ZnS as a shell and capped by 2-mercaptoethanol, which uses the thiol group to bind the Zn ions on the surface of core/shell QDs. Due to nontoxic nature of ZnS shell nanoparticles, these structures have application in determination of nucleic acids using the resonance light scattering method and biomolecular labelling [17] and have more potential applications such as solar cells [19], laser devices [20], light-emitting diodes [21], biological detection, electroluminescence devices, phosphors, optical sensors, optoelectronic devices and flat-panel displays [22]. For example, specific antibody-bound QDs can be used to image antigens on cellular, endothelial or mucosal surfaces in vivo [23], and fluorescence of antibody-linked QDs bound to the cancerous tissues in a mouse helped locate the tumour [24]. In addition, cellular proliferation can be quantified using a QD-based incorporation assay [25]. QDs have also been illustrated in molecular beacon to detect DNA [26–28]. We have employed X-ray diffraction (XRD), UV–Vis spectroscopy, photoluminescence spectroscopy, Fourier transform infrared spectroscopy (FTIR) and transmission electron microscopy (TEM) techniques to characterize ZnS, CdS and CdS/ZnS core/shell QDs to make sure that the prepared QDs can have applications in various above-mentioned fields. The originality and emphasis of our work are the formation of highly stable and luminescent bio-compatible wurtzite QDs via simple wet chemical method and the use of fewer selected chemicals at room temperature.

2 Experimental

2.1 Synthesis of CdS QDs

In the present work, CdS QDs were synthesized using wet chemical route at 35 ± 1 °C temperature. CdS nanoparticles were synthesized using cadmium chloride (Merck), ammonium chloride (Merck) and thiourea (Merck) as source material with distilled water as solvent. All chemicals were of analytical grade and used without further purification. The reaction matrix employed in our study consisted of $CdCl_2$, NH_4Cl and thiourea in 1:1.5:3 molar ratios. The reaction matrix was prepared in two parts. Cadmium chloride and ammonium chloride were mixed in 50 ml of distilled water. The pH was kept at 8.5 using liquid ammonia. Then, thiourea was added into 50 ml of prepared solution and continuously stirred, and immediately, 5 ml of 2-mercaptoethanol (5 %) was added to it in order to control the particle size of CdS QDs. The overall synthesis time was 5 h. The prepared nanoparticles appeared to be of crème colour. Prepared QDs were centrifuged (3,500 rpm, 10 min) and washed several times with distilled water before preservation.

2.2 Synthesis of ZnS QDs

The process for preparing ZnS QDs was similar to that of CdS QDs using wet chemical method at 35 ± 1 °C temperature. The reaction matrix employed in our synthesis consisted of AR grade $ZnSO_4$, $(NH_4)_2SO_4$ and thiourea in 1:1.5:1.5 molar ratios. Zinc sulphate dehydrates and ammonium sulphate were mixed in 50 ml of distilled water. The pH was kept at 9.5 using ammonia. Then, thiourea was dissolved in 50 ml of prepared solution. After that, a 5 ml of 5 % solution of 2-mercaptoethanol was added in this solution as surfactant and then continuously stirred for 5 h. Prepared QDs were centrifuged (3,500 rpm, 10 min) and washed several times with distilled water before preservation.

2.3 Synthesis of CdS/ZnS core/shell QDs

CdS/ZnS core/shell structures were synthesized by seed growth method. The reaction matrix employed in our study consisted of AR grade $ZnSO_4$, $(NH_4)_2SO_4$ and thiourea in 1:1.5:1.5 molar ratios. Zinc sulphate dehydrate and ammonium sulphate were mixed in 50 ml of distilled water. The pH was kept at 9.5 using ammonia. After this, processes prepared CdS solution was added (2.5 ml), and it

was followed by the addition of thiourea. After that, 5 ml of 5 % solution of 2-mercaptoethanol was added in solution as surfactant and continuously stirred for 5 h. At the end of the synthesis, prepared nanoparticles were collected by centrifugation (3,500 rpm, 10 min) and multiple washing with distilled water before preservation.

2.4 Characterization techniques

In order to study the different properties of the prepared quantum dots, we have characterized the samples using various techniques. Structural analysis has been performed using XRD, and the XRD patterns were recorded in a Shimadzu powder X-ray diffractometer using Cu Kα1 radiation. The optical properties were studied by Perkin-Elmer Lambda2 UV–Vis spectrophotometer, and absorbance spectra were recorded. Photoluminescence (PL) emission spectra of the samples were recorded by a computer-controlled rationing luminescence spectrophotometer LS55 (Perkin-Elmer Instruments, UK) with λ accuracy $= \pm 1.0$ nm and λ reproducibility $= \pm 0.5$ nm. A tunable 20 kW pulse <10 μs from a Xenon discharge lamp was used as the excitation source for recording photoluminescence emission spectra. A gated photo-multiplier tube was used as a detector. Prior to the PL experiments, signal-to-noise ratio was adjusted to 500:1, using the Raman band of water with excitation at 220 nm. The surface chemistry of the quantum dots has been studied using FTIR (Perkin-Elmer LS50). Transmission electron microscopy (Hitachi H-7500) has been performed as the finest proof for the particle size and particle size distribution.

3 Results and discussion

3.1 Structural analysis

In case of CdS and ZnS QDs, the selection of precursors and temperature plays an important role as it affects the crystal structure. Ramsden et al. [29] have also discussed that the dissolution of the precursors and interfacial forces might influence the lattice type of these QDs. It has been reported that the precursors of cadmium such as $CdCl_2$ and $Cd(NO_3)_2$ give a mixture of cubic and wurtzite phases. Milligan [30] has reported that the $CdCl_2$ favours the growth of wurtzite CdS. The effect of cadmium salt as well as sulphur as precursor plays important role on the structure of CdS and was studied by different groups [31 and references therein]. Hence, the selection of appropriate amount of $CdCl_2$ and thiourea as cadmium and sulphur precursors respectively near room temperature could give the wurtzite structure. Similar behaviour can be obtained in

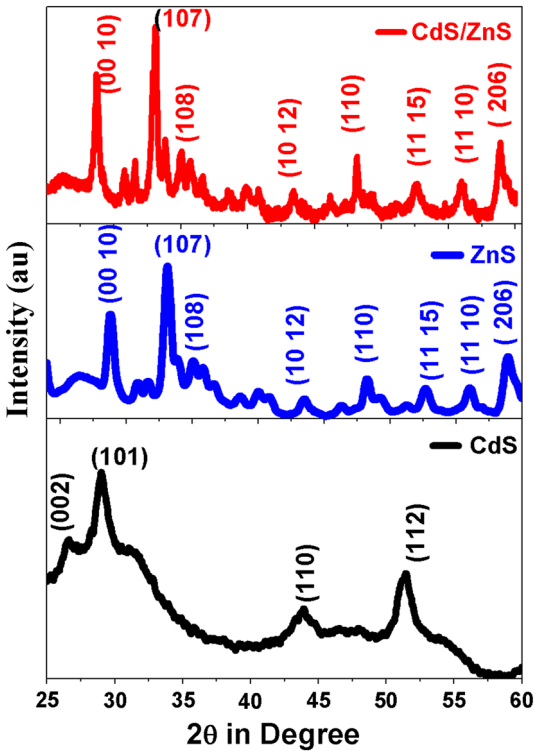

Fig. 1 Diffraction patterns of 2-mercaptoethanol capped CdS, ZnS and CdS/ZnS QDs

case of ZnS QDs based on selected precursor for Zn and S to form wurtzite structure near room temperature [32]. The formation of wurtzite CdS, ZnS and CdS/ZnS QDs has been studied by the means of XRD and discussed.

The XRD patterns of 2-mercaptoethanol capped smallest CdS, ZnS and CdS/ZnS QDs have been shown in Fig. 1. XRD analysis revealed that the crystal structure of CdS (Fig. 1) is wurtzite as the prominent peaks (26.5), (29.06), (43.8) and (51.6) were indexed to the wurtzite structure. There is broadening of these peaks in the spectra in comparison with bulk CdS, and this is due to the reduction in the crystallite size. The diameter (D) of the QDs has been calculated using Scherrer's formula [33].

$$D = \frac{k\lambda}{\beta \cos\theta} \quad (1)$$

where λ is the wavelength of the X-rays used, β the full width at half maximum of the 100 % XRD peak and θ the Bragg angle. The average crystallite size calculated for CdS QD is 4.2 nm, which was obtained from the width of the preferred (101) peak. The spectra of prepared ZnS QDs indicate the formation of wurtzite structure. The wurtzite-type structure was confirmed from the agreement of 2θ. The most prominent peak is oriented in (0 0 10) direction along with the other reflections at (107) and (205) planes. The average particle size was measured using Debye Scherer formula and found to be 5.2 nm. Significant

broadening in the peaks of ZnS spectra has been obtained attributing the formation of QDs. XRD pattern of CdS/ZnS core/shell structure indicates the formation of CdS/ZnS. In these spectra, most prominent peaks are similar to ZnS QDs, i.e. (0 0 10) direction along with the other reflections at (107) and (205) planes with a little shift in 2θ with respect to ZnS positions; also, there is shift in core/shell spectra with respect to CdS structure. The average particle size of CdS/ZnS core/shell was measured using Debye–Scherrer's formula and was found to be 5.8 nm.

The XRD analysis of ZnS and CdS/ZnS core/shell systems announced that the obtained crystal structures were wurtzite. This may be due to the use of organic materials basically the class of thiols in case of ZnS quantum dots that gets help to transform the phase of nanoparticles and hence in CdS/ZnS [34, 35]. As already mentioned, the XRD peak broadening could also be due to the strain in addition to the crystallite size of the particles [36]. Hence, an attempt has been made to estimate the strain (ε) of the prepared quantum dots using Stokes–Wilson equation.

$$\varepsilon_{\text{str}} = \beta/4\tan\theta \tag{2}$$

Lattice strain is a measure for the distribution of lattice constants arising from crystal imperfections, such as lattice dislocation. The other sources of strain are the grain boundary triple junction, contact or sinter stresses, stacking faults, coherency stresses, etc. In our study, it has been found that very minor strain occurs in QDs, and it shows QD structures are highly crystalline. CdS QDs have average strain, i.e. 0.73 ZnS; quantum dots have average strain i.e. 0.42 and core/shell structure have strain in between CdS and ZnS, i.e. 0.36. The broadening of XRD diffraction peaks normally comes from both dot size and strain, but these two effects can be separated as the size broadening does not depend on q vector, while the strain broadening does. It is not very accurate to extract size and strain independently from FWHM of XRD peaks, so we considered the well-known Hall–Williamson methods instead. The obtained results are presented in the Fig. 2. The obtained results from Hall–Williamson method support the findings from Scherrer's method and TEM analysis and have been tabulated in Table 1. All the structural parameters calculated from XRD data have been tabulated in Table 1, and it includes FWHM, intensity, phase assignment, lattice constant, strain and particle size of 2-mercaptoethanol capped CdS, ZnS and CdS/ZnS QDs at room temperature.

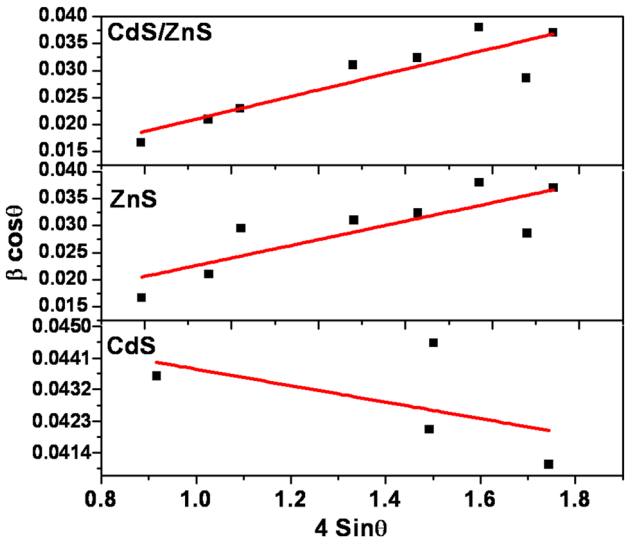

Fig. 2 Hall–Williamson plot for CdS, ZnS and CdS/ZnS QDs

3.2 Absorption spectroscopy

The UV–Visible spectra of the as-prepared CdS, ZnS and CdS/ZnS nanoparticles were shown in Fig. 3. Corresponding absorption edges due to the transition between electronic state in the conduction band and the hole state in the valance band have been exhibited around 435, 260 and 270 nm for CdS, ZnS and CdS/ZnS QDs, respectively, for the smallest QDs size in each case. A large blue shift about 0.50 eV in CdS and 0.80 eV in wurtzite ZnS QDs with respect to their bulk absorptions has been observed. The energy band gap for CdS, ZnS and CdS/ZnS QDs has been calculated from the corresponding absorption edges using the second derivative of the absorption spectra and using the formula

$$E_{\text{eV}} = hc/\lambda \tag{3}$$

where h = Planck's constant and E = energy band gap, λ = wavelength at absorption edge.

In 2-mercaptoethanol capped CdS QDs, absorption edge occurs at 435 nm and the band gap according to this edge is 2.9 eV in comparison with bulk which is 2.45 eV, and this is due to the reduction in particle size. Edge of capped ZnS QDs has been found at 260 nm with energy band gap of 4.5 eV compared to their bulk wurtzite form at 3.9 eV attributing the blue shift in band gap energy. The absorption edge of the core/shell structure lies between CdS and ZnS quantum dots at 270 nm because surface-to-volume ratio in core/shell is more than of CdS but less than ZnS. Consequently, discreteness of energy levels of core/shell should lie between CdS and ZnS. Based on this fact, the absorption edge of core/shell structure that is at 270 nm is between the edges of ZnS (260 nm) and CdS (435 nm). As some properties of quantum dots may be sensitive to the dot size, we have synthesized CdS, ZnS and CdS/ZnS quantum dots of different sizes and the obtained results are presented in the absorbance spectra (Fig. 3), as we can see there is the change in absorption edge according to the size of QDs. This continuous blue shift shows that quantum

Table 1 FWHM, intensity, phase assignment, lattice constant, strain and particle size of 2-mercaptoethanol capped CdS, ZnS and CdS/ZnS QDs at room temperature

Sample	2θ (degree)	d (Å)		FWHM (degree)	Intensity	(hkl)	Phase assignment	Particle size (D) Scherrer's (nm)	Particle size (D) Hall–Williamson (nm)	Lattice constant (Å)	Lattice mismatch (%)		Strain ε_{str} (Stokes–Wilson's)	Strain ε_{str} (Hall–Williamson's)
		Obs.	Sta.								a	c		
CdS	26.5	3.34	3.35	1.98	60	(002)	Wurtzite	4.2	2	$a = 4.2$, $c = 6.5$	0.2	0.2	0.99	0.002
	29	3.07	3.16	2.64	100	(101)	Wurtzite			$a = 4.1$, $c = 6.6$	0.2	0.1	1.19	
	43.8	2.06	2.07	1.86	22	(110)	Wurtzite			$a = 4.0$, $c = 6.3$	0.3	0.4	0.48	
	51.6	1.77	1.76	1.41	52	(112)	Wurtzite			$a = 4.1$, $c = 6.7$	0.4	0.1	0.27	
ZnS	28.7	3.1	3.16	0.99	6	(0010)	Wurtzite	5.1	3.8	$a = 3.82$, $c = 31.2$	0	0	0.45	0.020
	33.3	2.64	2.45	1.26	51	(107)	Wurtzite			$a = 3.82$, $c = 31.2$	0	0	0.47	
	35.5	2.51	2.45	1.78	23	(108)	Wurtzite			$a = 3.81$, $c = 31.2$	0.2	0	0.62	
	43.4	2.08	2.07	1.92	4	(1,012)	Wurtzite			$a = 4.04$, $c = 31.2$	5.7	0	0.24	
	48	1.9	1.89	2.03	7	(110)	Wurtzite			$a = 3.81$, $c = 31.2$	0.2	3.2	0.45	
	52.5	1.78	1.73	2.43	3	(1,015)	Wurtzite			$a = 3.82$, $c = 32.2$	0	0	0.46	
	56	1.66	1.67	1.86	6	(1,110)	Wurtzite			$a = 3.81$, $c = 31.2$	0.2	2.7	0.31	
	58	1.57	1.58	2.43	57	(205)	Wurtzite			$a = 3.82$, $c = 30.3$	0		0.38	
CdS/ ZnS	28.75	3.1	3.16	0.9	6	(0010)	Wurtzite	5.8	4.5	$a = 3.82$, $c = 31.2$	0	0	0.42	0.026
	33.34	2.64	2.45	1.19	51	(107)	Wurtzite			$a = 3.81$, $c = 31.2$	0.2	0	0.44	
	35.56	2.51	2.45	1.67	23	(108)	Wurtzite			$a = 3.82$, $c = 31.2$	0	0	0.53	
	43.47	2.08	2.07	1.79	4	(1,012)	Wurtzite			$a = 4.01$, $c = 32.2$	0.4	3.2	0.22	
	48.05	1.9	1.89	1.89	7	(110)	Wurtzite			$a = 3.82$, $c = 31.2$	0	0	0.39	
	52.53	1.78	1.73	2.21	3	(1,015)	Wurtzite			$a = 3.81$, $c = 31.2$	0.2	0	0.37	
	56.07	1.66	1.67	1.7	6	(1,110)	Wurtzite			$a = 3.82$, $c = 32.2$	0	3.2	0.22	
	58.04	1.57	1.58	2.35	57	(205)	Wurtzite			$a = 3.81$, $c = 0.34$	0.2	2.7	0.32	

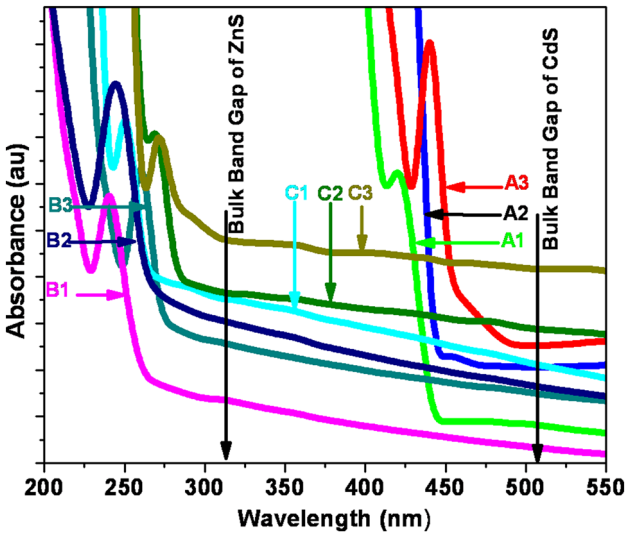

Fig. 3 Absorption spectra of 2-mercaptoethanol capped CdS (A1 < A2 < A3), ZnS (B1 < B2 < B3) and CdS/ZnS (C1 < C2 < C3) QDs (where the QD sizes are smallest for 1 and largest for 3)

Table 2 Particle size by EMA with corresponding blue shift of 2-mercaptoethanol capped CdS, ZnS and CdS/ZnS QDs at room temperature

Sample	Absorption edge (nm)	Band gap (eV)	Particle size by EMA	Energy band shift (eV)
CdS	435	2.9	3.4	0.5
ZnS	260	4.8	4.0	0.9
CdS/ ZnS	270	4.6	4.3	0.7 to ZnS band gap

confinement occurred in the prepared quantum dots and also the effectiveness of capping agent to obtain controlled size quantum dots. So we observed change in corresponding band edge absorption and will certainly get effective changes in other properties also. The particle size of smallest QDs of CdS, ZnS and CdS/ZnS calculated by EMA and band gap of those particles by virtue of reduction in size has been given in Table 2.

3.3 Photoluminescence spectroscopy

Schematic diagram for CdS/ZnS core/shell structure has been shown in Fig. 4. CdS/ZnS is type I core/shell structure in which the band gap of the shell is larger than that of the core. The conduction and valance band offsets are such that the conduction band of shell is higher than that of core, while the valance band of the shell is of lower energy than that of the core. This leads to an effective confinement of electron and hole in the core material. The exciton behaviour mechanism on the core/shell system and the emission of the fluorescent peaks are illustrated in Fig. 4.

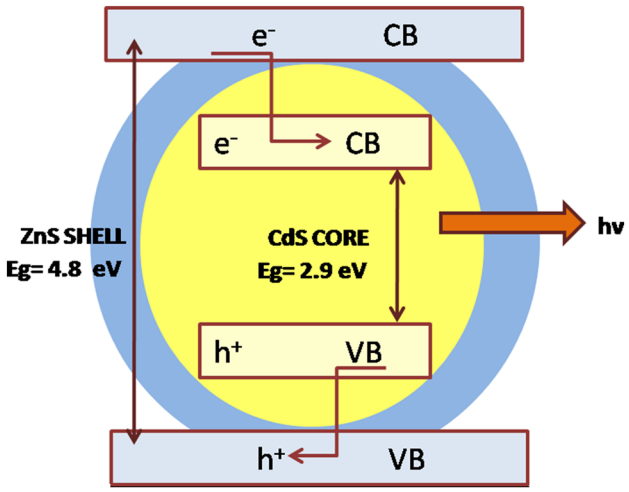

Fig. 4 Schematic diagram of CdS/ZnS core/shell structure

Applications of QDs would be restricted due to different nonradiative relaxations pathways. One of the most important nanoradiative pathways is surface-related defects. To overcome the above-mentioned difficulties, organic and inorganic capping agents are used to passivate the free quantum dots. The effect of using 2-mercaptoethanol as cappent has been studied for CdS, ZnS and CdS/ZnS core/shell structure and observed appealing results. The room-temperature PL spectra of 2-mercaptoethanol capped CdS, ZnS and CdS/ZnS for all QDs are shown in Fig. 5a, b. All the samples were excited at 220 nm, and the concentration of the solution was taken as 0.13 mg/ml for each sample for better comparison. The obtained results show that the 2-mercaptoethanol has an excellent capping efficiency because dangling bonds are effectively passivated. CdS QDs PL spectra originated from electrons in the conduction band, excitonic states and trap states [37–39]. In the case of CdS QDs, it was reported [40, 41] that the energy emission band at 350–500 nm was due to the radiative recombination of free charge carriers or excitonic fluorescence, while PL peak at 500–700 nm was attributed to the recombination of charge carriers in deep traps of surface-defect states.

As seen in spectrum 5-A, the emission peak of the CdS QDs sample is located at 540 nm, which presents blue shift compared to bulk CdS at 650 nm [42]. It is obvious that the recombination of charge carriers in deep traps of surface-defect states is responsible for the observed PL spectra. PL peak centred at 437 nm shows ZnS spectra, as shown in Fig. 5b. Peak at 437 nm was derived from the near-band-edge recombination of the free excitons of ZnS [43]. It is also termed as self-activated luminescence and is known to be due to the recombination of carriers between the sulphur vacancy-related donor and the valence band [44]. The emission spectra of ZnS QDs are having comparatively 2.5-

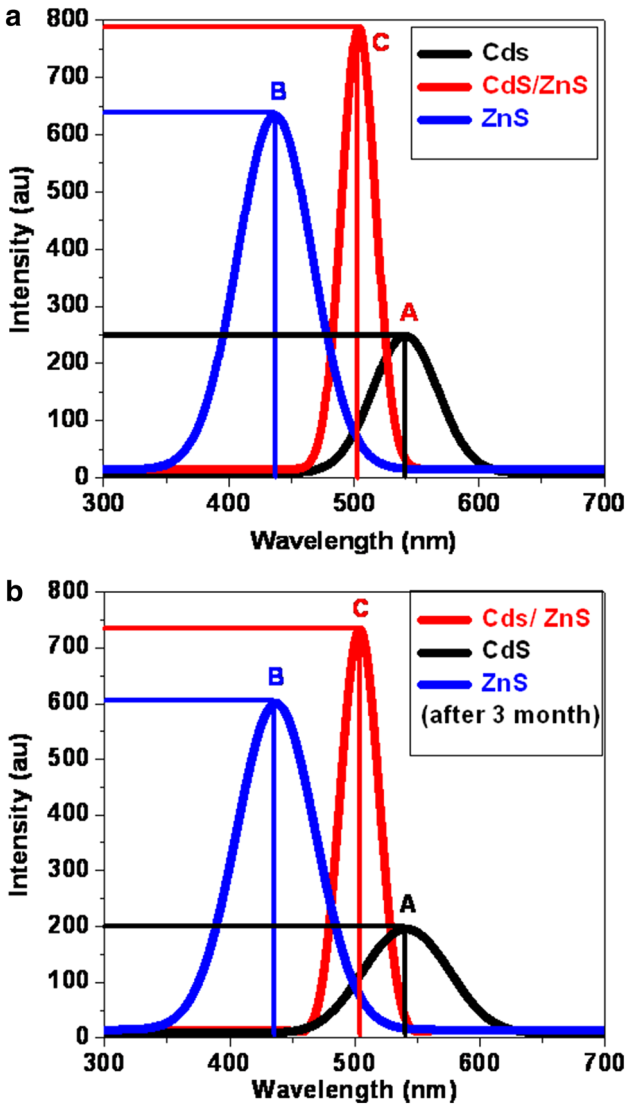

Fig. 5 Room-temperature photoluminescence spectra of 2-mercaptoethanol capped CdS-A, ZnS-B and CdS/ZnS-C QDs **a** for fresh samples and **b** for 3-month-aged samples

Table 3 Comparison of photoluminescence emission intensity and FWHM for CdS, ZnS and CdS/ZnS quantum dots

Sample name	Particle size by XRD (nm)	Emission peak			Increment in intensity (in folds)
		Intensity	FWHM	Wavelength (nm)	
CdS	4.2	250	61	540	1.0
ZnS	5.1	635	80	437	2.5
CdS/ ZnS	5.8	785	34	505	3.0

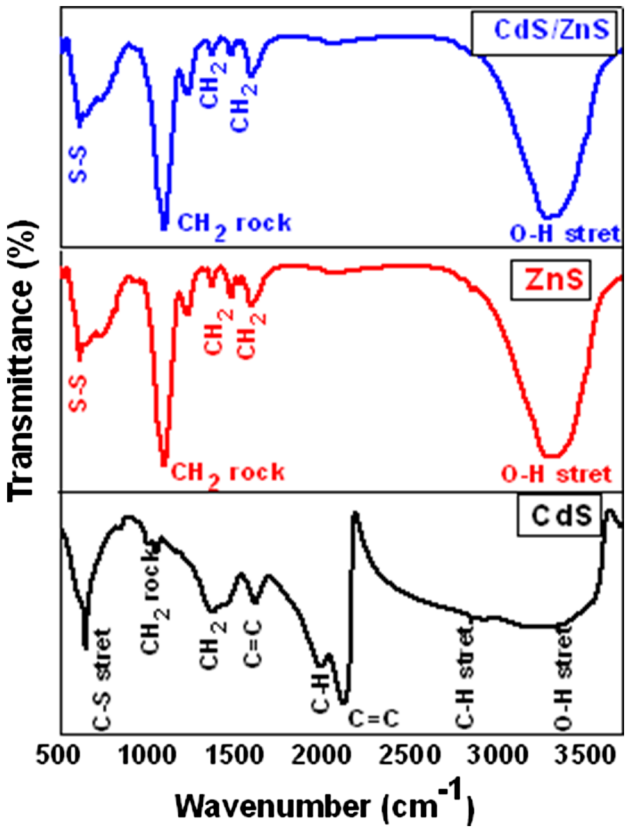

Fig. 6 FTIR spectra of 2-mercaptoethanol capped CdS, ZnS and CdS/ZnS quantum dots

fold enhancement from CdS because ZnS is optically transparent to the emission range; therefore, there are no photon losses associated with the ZnS shell with visible light emission [45]. The formation of ZnS shell can greatly passivate the core surface to protect it from oxidation and prevent CdS leaching into the surrounding medium and also improve the photoluminescence yield and photo-stability [46–48]. Interesting result of the work can be seen from the PL emission spectra 5-C for the capped CdS/ZnS structure, which is significantly high in comparison with capped CdS and ZnS nanoparticles. There were around threefold increment in intensity when we go from CdS to CdS/ZnS structure. This is because core/shell nanoparticles are excited, and the photo-induced charge carriers migrate to the interface and trap in the misfit dislocations. Therefore, the emissions observed can be attributed to the radiative recombination of carrier at CdS/ZnS interface. Due to these factors, core/shell structures gives more enhanced luminescence. The full width at half maxima of PL emission peaks was found to be 61, 80 and 34 nm for CdS, ZnS and CdS/ZnS systems, respectively, and the results have been tabulated in Table 3. This shows the effective tunability with narrow emission, and hence, there was increment in the monochromaticity of the prepared CdS/ZnS structure. Stability testing provides evidence on how the quality of the sample varies with time under the influence of a variety of environmental conditions, such as temperature, humidity

and light. In order to test the stability in prepared samples, we have gone through a procedure. CdS, ZnS and CdS/ZnS samples were prepared initially in consecutive 2 days and were preserved in distilled water in a closed vial in normal atmospheric conditions in a clean bench away from direct sunlight. Fresh samples were prepared in summers (room temperature 32–34 °C), and PL spectra have been recorded immediately. To test the stability, the PL spectra of stored samples have been recorded again after 3 months at that time the room temperature was 20–22 °C. Three-month-aged samples of CdS, ZnS and CdS/ZnS as shown in Fig. 5b have also been analysed, and it confers approximately the same luminescence as fresh sample. It indicates that there is no more agglomeration exists in the QDs on ageing, and a stable wurtzite structure has been attained. As it is clear from the Fig. 5b, there is negligible change in emission intensity in all the samples; hence, results indicate the effectiveness of the synthesis procedure and the use of capping agent to stabilize the QDs.

3.4 FTIR analysis

2-Mercaptoethanol capped CdS, ZnS and CdS/ZnS quantum dots were examined by recording their FTIR spectra in the range 4,500–400 cm^{-1} (Fig. 6). The broad peaks in CdS QDs obtained at 3,400, 1,383 and 667 cm^{-1} and weak peaks at 2,917, 1,053 and 1,055 cm^{-1} were assigned to O–H, CH_2, C–S and C=C and for weak peaks O–H, CH_2–OH and CH_2, respectively, in the CdS sample as shown in the spectra. The sharp peak at 3,400 and 667 cm^{-1} corresponds to (O–H) alcohol along with small peaks at 2,917 cm^{-1} for (C–H) stretching alkanes and 1,053, and 1,055 cm^{-1} for O–H means carboxylic acid and CH_2 rock alkanes. Since the surface capping of sulphide particles by thiols is attributed to coordination of the mercapto groups to the sulphide surfaces, these IR spectra strongly confirm the surface capping of the CdS nanoparticles by direct bonding of the mercapto group of 2-mercaptoethanol.

These results also suggest that the primary hydroxyl groups at the other end of the capping thiol can serve as a surface hydrophilic moiety of the capped CdS nanoparticles, and H_2O might be adsorbed more readily on the modified sulphide surfaces, respectively [49]. In case of ZnS and CdS/ZnS core/shell structures, similar peaks were found because both systems possess same surface chemistry. These results show how effectively ZnS covers the CdS core and reduce the toxicity of CdS materials as ZnS is nearly nontoxic for biomolecules. Passivation of CdS by ZnS has been confirmed by the formation of S–S bond (400–600 cm^{-1}), which occurs due to breaking of S–H bonds. S–S bond arises between sulphur from thiol group existing in the capping agent and sulphur in the ZnS QDs also shows CH_2 which exists at 1,470–1,300 cm^{-1} as reported. Functional groups that are present on QDs surface have been tabulated in Table 4. This peak shifts to 1,396 cm^{-1} for 2-mercaptoethanol capped ZnS QDs and core/shell in our case. The functional groups that are present on the surface of the prepared samples can be easily attached with biomolecules. Generally, OH (hydroxyl), COOH (carboxylic acid) or amine functionalities are present on the biomolecules surfaces [50, 51], and similar functional groups are present in ours the as-prepared QDs. So that prepared QDs have compatibility to attach with biomolecule. ZnS present at the shell that is nontoxic and gives more opportunity to apply CdS/ZnS structure for bio-application like bio-imaging.

Here, one important point is worth mentioning that, as we have opted for aqueous medium to prepare luminescent QDs, as the results there is always hydrophilic surfaces of QDs which are directly conjugatable to bio-molecules. This is an affirmative aspect of our technique as we can use these as-prepared water soluble QDs directly but the QDs obtained by high-temperature organic synthesis routes are always possessing hydrophobic surfaces. Therefore, there is a strong need for hydrophobic surface modification of nanocrystals using surface exchange of the hydrophilic coordinating solvent with commonly used hydrophilic thiol acids such as mercaptopropionic acid (MPA) or mercaptoethanol (ME) [52, 53] before bioconjugation with their functional groups.

Table 4 List of functional groups present on the surface of QDs capped with 2-mercaptoethanol

Type of vibrations (cm^{-1})	Peaks (cm^{-1})	CdS with 2-mercaptoe thanol (cm^{-1}) in prepared QDs	ZnS, CdS/ZnS with 2-mercaptoethanol (cm^{-1}) in prepared QDs
O–H stretching	3,300	3,400	3,400
C–H stretching, CH_2 asymmetric	2,936–2,916	2,917	
CH_2 wagging	1,347–1,182	1,383	1,396, 1,251
Alcohol CH_2–OH, C–O primary stretching	1,075–1,000	1,053	1,114
CH_2 rock	1,174–724	1,055	
C–S stretching	705–570	667	657, 618

3.5 Transmission electron microscopy

Transmission electron microscopy has been employed to ensure about the particle size and to check the effectiveness of cappent, and the results for CdS, ZnS and CdS/ZnS QDs are presented in Fig. 7. TEM image (Fig. 7a) of the CdS QDs shows highly monodispersed nanoparticles with average sizes of 5.3 nm as vindicated from the corresponding histogram. Similarly, ZnS QDs (Fig. 7b) have particle size of 5.8 nm, and CdS/ZnS QDs (Fig. 7c) have particle size of 6.2 nm. It is also clear from the figure that there is no agglomeration of QDs, and we can obtain either the fine solution or even powder of uniformly distributed nanoparticles for various applications. The FWHM of TEM histograms for all 3 kinds of quantum dots has the values, i.e. 2.4 nm for CdS, 3.4 nm for ZnS and 1.6 nm for CdS/ZnS. This result clearly shows that the size dispersion has been controlled on the formation of CdS/ZnS core/shell structures. To reduce QD's size dispersion, we have optimized the synthesis conditions such as reaction temperature, reaction duration, pH, selection of precursor materials and their ratio and appropriate time to add cappent in the running reactions and core/shell structure formation.

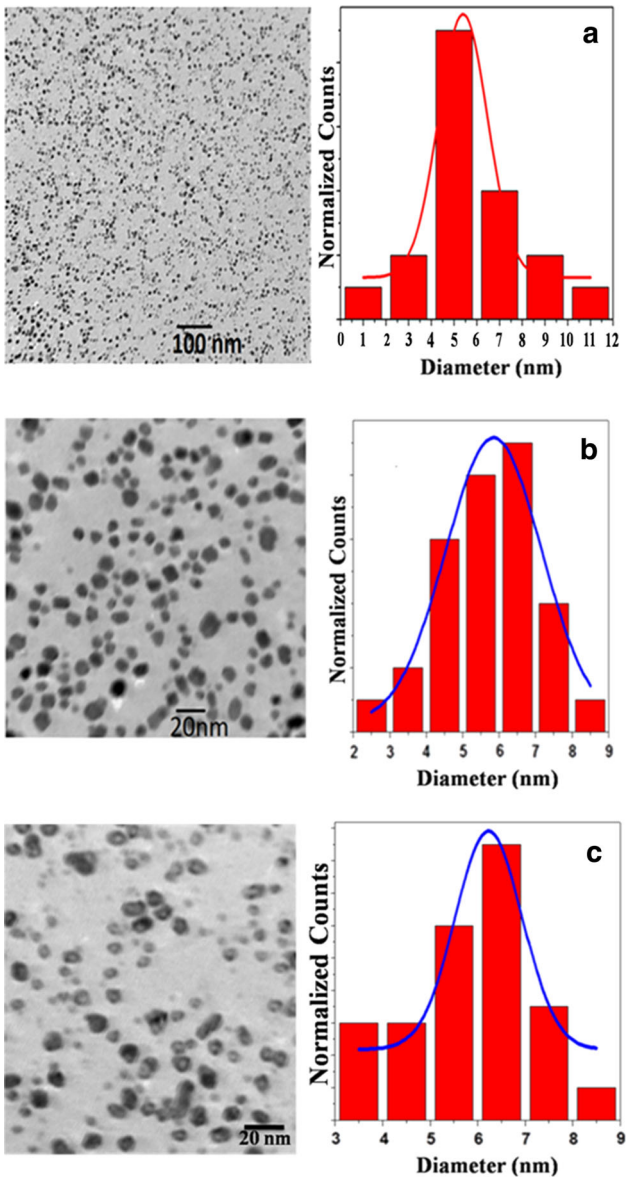

Fig. 7 TEM image of QDs and their particle size distribution for **a** CdS, **b** ZnS and **c** CdS/ZnS

Table 5 Particle sizes obtained from EMA, XRD and TEM for CdS, ZnS and CdS/ZnS QDs at room temperature

Sample	Particle size by EMA (nm)	Particle size by XRD (nm)	Particle size by TEM (nm)
CdS	3.4	4.2	5.3
ZnS	4	5.1	5.8
CdS/ZnS	4.3	5.8	6.2

Particle sizes obtained from absorption, XRD and TEM have been tabulated in Table 5. The particle size calculated from effective mass approximation using absorption data is comparable to the size obtained from XRD data, whereas the particle sizes obtained from TEM are slightly greater than the size obtained from XRD analysis. The size obtained by XRD and TEM has the correlation that the XRD size is usually equals or smaller than the size obtained by TEM [54]. When the particles are delineated by well defined boundary or in the form of loose nanoparticles of materials as shown in Fig. 7, XRD and TEM values are in good agreement. In bulk nanocrystalline materials produced by various methods, the XRD result is usually smaller than TEM size. On the other hand, in nanocrystalline materials, the term grain is used interchangeably with crystallite to refer to the smallest single-phase and crystallized regions separated by grain boundaries. Each crystallite is itself a "single crystal" as such; it can contain any or all of the zero-, one-, or two-dimensional defects except for grain boundaries, interphase boundaries and surfaces. In the case where the particle is single crystal nanoparticles the crystallite size and particle size is identical. As we can see from Table 5, there is no big difference in the particle sizes obtained from different techniques, and it clearly shows that the as-prepared nanoparticles have no agglomeration.

4 Conclusions

Highly stable, luminescent, nearly monodispersed wurtzite CdS, ZnS and CdS/ZnS QDs structures were successfully

synthesized through wet chemical method, and their structural as well as optical properties were investigated by XRD, UV–Vis spectroscopy, photoluminescence spectroscopy, FTIR and TEM. XRD results indicated that synthesised QDs have lower grain size and less strained particles. The particle sizes of CdS, ZnS and CdS/ZnS QDs as determined from XRD and TEM were in good agreement. The UV–Visible spectra show a large blue shift attributing to the enhanced optical properties; this is the size-dependent blue shift of absorption edge and attributed to the quantum size effect. PL measurement shows effectiveness of capping agent and core/shell structure formation as there is clear vindication of significantly enhanced luminescence efficiency. Highly monodispersed CdS, ZnS and CdS/ZnS core/shell nanocrystals with high quantum yield and narrow PL spectra have been obtained. FTIR results show the effect of ZnS as a shell and 2-mercaptoethanol as capping agent in core/shell structure formation and vindicate our ability to synthesise biocompatible QDs. This method can also be relevant to synthesize the other core/shell semiconductor nanocrystals.

References

1. M. Nirmal, L. Brus, Acc. Chem. Res. **32**, 407 (1999)
2. A.P. Alivisatos, Science **271**, 933 (1996)
3. H. Weller, Angew Chem. Int. Ed. Engl. **32**, 41(1993)
4. U. Banin, Y.W. Cao, D. Katz, O. Millo, Nature **400**, 542 (1999)
5. M. Bruchez, M. Moronne, P. Gin, S. Weiss, A.P. Alivisatos, Science **281**, 2013 (1998)
6. W.C.W. Chan, S. Nie, Science **281**, 2016 (1998)
7. G.P. Mitchell, C.A. Mirkin, R.L. Letsinger, J. Am. Chem. Soc. **121**, 8122 (1999)
8. K. Rajeshwar, de R. Tacconi, C.R. Chenthamarakshan, Chem. Mater. **13**, 2765 (2001)
9. A.P. Alivisatos, Science **271**, 933 (1996)
10. M.A. Anderson, S. Gorer, R.M. Penner, J. Phys. Chem. B **101**, 5895 (1997)
11. G. Henshaw, I.P. Parkin, G. Shaw, Chem. Commun. **10**, 1095 (1996)
12. T. Hirai, Y. Bando, I. Komasawa, J. Phys. Chem. B **106**, 8967 (2002)
13. M. Kuno, J.K. Lee, B.O. Dabbousi, F.V. Mikulec, M.G. Bawendi, J. Chem. Phys. **106**, 9869 (1997)
14. B.O. Dabbousi, J. Rodriguez-Viejo, F.V. Mikulec, J.R. Heine, H. Mattoussi, R. Ober, K.F. Jensen, M.G. Bawendi, J. Phys. Chem. B **101**, 9463 (1997)
15. X. Peng, M.C. Schlamp, A. Kadavanich, A.P. Alivisatos, J. Am. Chem. Soc. **119**, 7019 (1997)
16. F. Zuoling, Z. Shihong, S. Jinsheng, Z. Siyuan, Mater. Res. Bull. **40**, 1591 (2005)
17. B. Liu, G.Q. Xu, L.M. Gan, C.H. Chew, W.S. Li, Z.X. Shen, J. Appl. Phys. **89**, 1059 (2001)
18. P.K. Sahoo, S.S. Kamal Kalyan, T. Kumar Jagadeesh, B. Sreedhar, A.K. Singh, S.K. Srivastava, Def. Sci. J. **59**(4), 447 (2009)
19. W.C.W. Chan, S.M. Nie, Science **281**, 2016 (1998)
20. W.U. Huynh, J.J. Dittmer, A.P. Alivisatos, Science **295**, 2425 (2002)
21. H.J. Eisler, V.C. Sundar, M.G. Bawendi, M. Walsh, H.I. Smith, V. Klimov, Appl. Phys. Lett. **80**, 4614 (2002)
22. M.C. Schlamp, X.G. Peng, A.P. Alivisatos, J. Appl. Phys. **82**, 5837 (1997)
23. T. Yamamoto, S. Kishimoto, S. Lida, Phys. B **308**, 916 (2001)
24. C. Seydel, Science **30**, 80 (2003)
25. C.S. Wu, M.K.K. Oo, J.M. Cupps, X. Fan, Biosens. Bioelectron. **26**, 3870 (2011)
26. C.Y. Zhang, J. Hu, Anal. Chem. **82**, 1921 (2010)
27. N.C. Cady, J.W. Lee, R.S. Foote (eds.), *Micro and Nanotechnology in Bioanalysis: Methods and Protocols* (Springer, Berlin, 2009), pp. 544, 367
28. J.H. Kim, S. Chaudhary, M. Ozkan, Nanotechnology **18**, 195105 (2007)
29. J.J. Ramsden, S.E. Webber, M. Gratzel, J. Phys. Chem. **89**, 2740 (1985)
30. M.O. Milligan, J. Phys. Chem. **38**, 797 (1934)
31. N. Ghows, M.H. Entezari, Ultrason. Sonochem. **18**, 269 (2011)
32. C. Yuanrong, L. Zhe, L. Hao, Z. Liang, Y. Bai, Nanotechnology **25**, 115601 (2014)
33. B.D. Cullity, *Elements of X-Ray diffraction* (Addison-Wesley Publishing Company Inc., London, 1978)
34. A. Rahdar, J. Nanostructure Chem. **3**, 10 (2013)
35. P. Thangadurai, S. Balaji, P.T. Manoharan, Nanotechnology **19**, 435708 (2008)
36. A. Mercy, R. Samuel Selvaraj, B. Milton Boaz, A. Anandhi, R. Kanagadurai, Indian J. Pure Appl. Phys. **51**, 448 (2013)
37. A. Sengupta, B. Jiang, K.C. Mandal, J.Z. Zhang, J. Phys. Chem. B **103**, 3128 (1999)
38. M.C. Brelle, J.Z. Zhang, L. Nguyen, R.K. Mehra, J. Phys. Chem. A. **103**, 10194 (1999)
39. C. Unni, D. Philip, K. Gopchandran, Spectrochim. Acta A. **71**, 1402 (2008)
40. N. Chestnoy, T.D. Harris, R. Hull, L.E. Brus, J. Phys. Chem. **90**, 3393 (1986)
41. B.C. Zhang, Y.H. Shen, A.J. Xie, L.B. Yang, X.F. Wang, Mater. Chem. Phys. **116**, 392 (2009)
42. Y.C. Cao, J.H. Wang, J. Am. Chem. Soc. **126**, 14336 (2004)
43. Z. Yang, Z. Zuo, H.M. Zhou, W.P. Beyermann, J.L. Liu, J. Cryst. Growth **314**, 97 (2011)
44. K. Jayanthi, S. Chawla, H. Chander, Cryst. Res. Technol. **10**, 976 (2007)
45. B.O. Dabbousi, J. Rodriguez-Viezo, F.V. Mikulec, J. Phy. Chem. B. **101**, 9463–9475 (1997)
46. I.L. Medintz, H.T. Uyeda, E.R. Goldman, H. Mattoussi, Nat. Mater. **4**, 435 (2005)
47. M.A. Hines, P.T. Guyotsionnes, J. Phys. Chem. **100**, 468 (1996)
48. X.G. Peng, M.C. Schlamp, A.V. Kadavanich, A.P. Alivisatos, J. Am. Chem. Soc. **119**, 7019 (1997)
49. H. Fujii, K. Inata, M. Ohtaki, K. Eguchi, H. Arai, J. Mater. Sci. **36**, 527–532 (2001)
50. K.S. Siow, L. Britcher, S. Kumar, H.J. Griesser, Plasma Process. Polym. **3**, 392 (2006)
51. R.A. Sperling, W.J. Parak, Phil. Trans. R. Soc. A **368**, 1333–1383 (2010)
52. W.C. Chan, S. Nie, Science **281**, 2016 (1998)
53. S.F. Wuister, I. Swart, F.V. Driel, S.G. Hickey, C. Donega, Nano Lett. **3**, 503 (2003)
54. J. Gubicza, G. Tichy, T. Ungára, Powder Diffr. **20**(4), 366 (2005)